Hydrol. Earth Syst. Sci. Discuss., 7, 1589–1619, 2010
www.hydrol-earth-syst-sci-discuss.net/7/1589/2010/


Hydrology and Earth System Sciences Discussions

This discussion paper is/has been under review for the journal Hydrology and Earth System Sciences (HESS). Please refer to the corresponding final paper in HESS if available.

# Spatial variability in floodplain sedimentation: the use of generalized linear mixed-effects models

**A. Cabezas**[1,2], **M. Angulo-Martínez**[3], **M. Gonzalez-Sanchís**[1], **J. J. Jimenez**[1], **and F. A. Comín**[1]

[1]Pyrenean Institute of Ecology-Spanish Research Council, IPE-CSIC. 1005 Avd. Montañana, 50080 Zaragoza, Spain
[2]Leibniz-Institute of Freshwater Ecology and Inland Fisheries, Berlin, Germany, IGB, Müggelseedamm 310, 12587 Berlin, Germany
[3]Aula Dei Experimental Station – Spanish Research Council, EEAD-CSIC. 1005 Avda. Montañana, 50080 Zaragoza, Spain

Received: 10 February 2010 – Accepted: 22 February 2010 – Published: 26 February 2010

Correspondence to: A. Cabezas (acabezas@ymail.com)

Published by Copernicus Publications on behalf of the European Geosciences Union.

## Abstract

Sediment, Total Organic Carbon (TOC) and total nitrogen (TN) accumulation during one overbank flood (1.15 y) were examined at one reach of the Middle Ebro River (NE Spain) for elucidating spatial patterns. To achieve this goal, four areas with different geomorphological features and located within the study reach were examined by using artificial grass mats. Within each area, 1 $m^2$ study plots consisting on three pseudo-replicates were placed in a semi-regular grid oriented perpendicular to the main channel. TOC, TN and Particle-Size composition of deposited sediments were examined and accumulation rates estimated. Generalized linear mixed-effects models were used to analyze sedimentation patterns in order to handle clustered sampling units, specific-site effects and spatial self-correlation between observations. Our results confirm the importance of channel-floodplain morphology and site micro-topography in explaining sediment, TOC and TN deposition patterns, although the importance of another factors as vegetation morphology should be included in further studies to explain small scale variability. Generalized linear mixed-effect models provide a good framework to deal with the high spatial heterogeneity of this phenomenon at different spatial scales, and should be further investigated in order to explore its validity when examining the importance of factors such as flood magnitude or suspended sediment solid concentration.

## 1 Introduction

Riverine floodplains can buffer the transport of sediment as washload mobilised from the upstream parts of the catchment. Such sediment deposition over floodplains is an important process in the storage and cycling of sediments, nutrients and contaminants in the river basins (Walling and Nicholas, 1996; Steiger and Gurnell, 2003; Walling and Owens, 2003; Noe and Hupp, 2009). Focussing on organic carbon (TOC) and nitrogen (TN), deposition during overbank floods is an important ecosystem function which provides important benefits as water quality enhancement or mitigation of greenhouse effect (Johnston, 1991; Day et al., 2004; Verhoeven et al., 2006, IPCC, 2007). At reach scale, TOC and TN ex-change between the main channel and its adjacent floodplain plays a key role on the ecological functioning (Junk, 1999; Tockner et al., 1999, 2000, Knosche, 2006; Preiner et al., 2008). Previous research has shown how human-induced changes at basin and reach scale have decreased the potential of riverine floodplains to act as sediment-associated nutrient sinks (Noe and Hupp, 2005; Owens et al., 2005; Pierce and King, 2008; Cabezas et al., 2009b; Cabezas and Comin, 2010). To accomplish knowledge-based management and restoration strategies at specific river reaches, TOC and TN deposition patterns must be properly understood.

The amounts and patterns of overbank sedimentation depend on several factors, namely frequency and duration of inundation, suspended sediment concentration in the main channel, and the flow patterns and stream velocity during floods (Allen, 1985). Regarding to individual events, hydraulic connectivity determines the loading rate of material over floodplains. Hydraulic connectivity, in turn, is controlled at reach scale by channel-floodplain geomorphology, which promotes spatial variability on sedimentation load and patterns for a given river section during a specific flood event (Hupp, 2000; Steiger and Gurnell, 2003; Noe and Hupp, 2005; Piegay et al., 2008). At this scale, previous studies have indicated that distance from the main channel exerts more influence on spatial variability of overbank sedimentation than downstream variation (Walling and He, 1998; Middlekoop and Asselman, 1998). Such trends were also observed at specific floodplain sections – site-scale – with uniform relief. At more complex sites, however, heterogeneity was strongly related with site micro-topography since it controls flow hydraulics, and thus suspended sediment transport and deposition (Nicholas and Walling, 1997). With regards to TOC and TN, the amount of sediment deposited and particle-size composition seem to determine the TOC and TN deposited in situ during overbank floods (Asselman and Middlekoop, 1995; Walling and He, 1997; Steiger and Gurnell, 2003).

In this context, different modelling approaches have been performed in order to gain a better understanding on sedimentation processes and predicting flood effects. Earlier numerical modelling research focussed on diffusive sediment and grain-size deposition across channel and floodplain sections (James, 1985; Pizzuto, 1987). By coupling hydraulic and sediment deposition models, field-based sedimentation rates and digital elevation models of the floodplain surface were incorporated to numerical modelling in order to reflect the high spatial heterogeneity observed in field-based investigations. Some of these models are based on a discrete-element approach (Stewart et al., 1998; Buttner et al., 2006), and other models on a finite-element approach (Nicholas and Walling, 1997, 1998; Middlekoop and Van der Perk, 1998). Those techniques allowed improving the knowledge in sedimentation trends predicted by simple, computationally efficient functions parameterised by distance from the main channel and floodplain elevation. It also allows the inclusion of the effect of meso-scale topographic features as abandoned channels, levees or drainage ditches (Nicholas and Mitchell, 2003).

However, empirical studies on contemporary sediment deposition are still needed to gain insight in the key variables that determine spatial heterogeneity (Walling et al., 2004). Previous studies have shown that spatial variability on sediment deposition is also high at smaller spatial scales – 1 $m^2$ – (Steiger and Gurnell, 2003; Steiger et al, 2003) where sediment traps were laid on clusters. Generalized linear mixed-effect models (GLME) provide a framework are able to handle clustered data by estimating cluster-specific random effects and introducing correlated residual structures (Pinheiro and Bates, 2000; Heegaard and Nilsen, 2007). Also differences at different floodplain sections and the self-correlation between observation points lying within the same section (Middlelkoop and Asselman, 1998; Steiger and Gurnell, 2003) can be included in this statistical model (Witherington et al., 2009).

In this paper, we apply a novel approach to analyze sediment, TOC and TN deposition patterns on one reach of the Ebro River during one individual flood. By using mixed-effect models, the effect of random variability and spatial correlation was considered in deposition modelling, apart to other factors as distance from the main channel, particle-size composition or site effects. Therefore, the objectives of such analysis were focused on: i) elucidate driving factors promoting spatial variability on sediment, TOC and TN deposition at different spatial scales and ii) evaluate the use of mixed-effect models for sedimentation studies at reach scale as a tool to deal with spatial variability at smaller scales.

## 2 Materials and methods

### 2.1 Study reach

The study reach (Fig. 1) is located in the Middle Ebro River (NE Spain), which is the largest river in Spain – watershed area = 85.362 $km^2$; river length = 910 km; average annual discharge to the Mediterranean Sea = 14.442 $Hm^3$; 1927–2003. Within this section, the average floodplain width is about 5 km (Ollero, 1995). The main channel has a wandering morphology – sinuosity = 1.39; mean channel slope = 0.050%; mean channel width = 110.31±36.3 m – with elongated meanders and scarcity of in-channel islands. Within the reach studied, the daily average discharge is 228.24 $m^3 s^{-1}$ – 1927–2007 – and the elevation ranges between 175 m a.s.l. in the river channel to 185 m a.s.l. at the base of the scarp. At the Zaragoza city gauging station – A011 at www.chebro.es, 12 km upstream the study reach – the potential storage capacity is 1.637.19 $hm^3$, impounding about 50% of the mean annual runoff. Regarding to landscape composition, agricultural fields have increasingly dominated over natural patch types since 1957, whereas lateral migration of main channel no longer takes place since 1981 (Cabezas et al., 2009).

### 2.2 Sediment sampling and analyses

Sediment traps were used to collect the sediment deposited by a single flood – 27 days – on March 2007, which reached 1624 $m^3 s^{-1}$ – 1.15 y, 1927–2003; 2.73 y, 1981–2003 – at the Zaragoza gauge station – A011 in www.chebro.es; 12 km upstream from the study area. The sediment traps were placed in four sites with different geomorphological traits and superficial connectivity – Fig. 1, Table 1: Mejana de Pastriz (MP) and

Margen Derecha (MD), with higher superficial connectivity than Soto del Francés (SF) and Rincón Falso (RF). At each area, 1 $m^2$ plots – $p$=15 at MP, MD and SF; $p$=22 at RF – were placed in a semi-regular grid, consisting of several transects – $t$=3 at MP, MD and SF; $t$=5 at RF – that were oriented perpendicular to the main stream (Fig. 2). The shape and size of each area directed the space between transects and between plots. Study plots were marked by digging a metallic stick, which was geo-referenced using a differential GPS device – Top-Com®, ±2 cm. In each plot, three 25×25 cm sediment traps – pseudo-replicates – made of artificial grass mats – $i$=201 – which had been previously weighed, were affixed to the surface using 14 cm steel pins at 30 cm on the left, right and opposite-to-the-river places around the metallic sticks. For each pseudo-replicate, three geographical variables were considered: i) elevation a.s.l. (m), extracted from the GPS device measurements; ii) perpendicular distance (m) to the main channel; and iii) longitudinal distance, calculated as the distance to the zone where superficial inputs enters during overbank floods (Fig. 1), which is located at the upstream part of each site ($j$=4) and was previously identified from field-based knowledge. Both perpendicular and longitudinal distances were estimated using ArcGIS 9.2®

A few days after the flood event, when all of the mats had re-emerged, they were taken to the lab and air-dried at lab temperature. Only 3.99% of the artificial grass mats were flushed away by the river. Sedimentation rates were calculated as sediment dry mass per area unit (kg $m^{-2}$) after re-weighing each sediment trap. Afterwards, a sediment sample was removed from each trap by hand using a brush with metallic bristles. All sediment samples were finer than 2 mm, so no sieving was necessary. An aliquot was separated for particle-size analysis with a laser-diffraction instrument (Coulter LS 230, Beckman Coulter®). The <4 µm, <63 µm, <125 µm, <250 µm and <500 µm particle-size separates were considered for further analyses. Such separates cumulatively represent the clay, silt, and very fine sand, fine sand and medium sand fractions according to Weinthwork (1922). The sediment samples were grounded with a mortar and pestle prior to measure Total Organic Carbon (TOC) and Total Nitrogen (TN) using elemental analysis (Leco SC-144DR® and Elementar Variomax CN®, respectively). TOC (g C $m^{-2}$) and TN (g N $m^{-2}$) accretion rates were calculated multiplying by sedimentation rates.

### 2.3 Spatial heterogeneity at reach scale

To describe spatial variability at reach scale, inter-site ($j$=4) differences on TOC (%, g C $m^{-2}$), TN (%, g N $m^{-2}$), particle size-class separates (% <4, 63, 125, 250, 500 µm) and sedimentation rates (kg $m^{-2}$) were explored. After ensuring that data met the assumption of normality (including transformations where appropriate), a one-way ANOVA was performed using SPSS® 14.0. Depending on the homogeneity of the variance, either SNK or Tahmane Tests were used in post-hoc comparisons. To describe spatial variability at reach scale, inter-site ($j$=4) differences on TOC (%, g C $m^{-2}$), TN (%, g N $m^{-2}$), particle size-class separates (% <4, 63, 125, 250, 500 µm) and sedimentation rates (kg $m^{-2}$) were explored. After ensuring that data met the assumption of normality (including transformations where appropriate), a one-way ANOVA was performed using SPSS® 14.0. Depending on the homogeneity of the variance, either SNK or Tahmane Tests were used in post-hoc comparisons.

The existence of spatial self-correlation was tested for the three variables by finding the most appropriate semi-variogram models to fit the empirical semi-variograms computed from the samples. The R statistical analysis system—function *variogram* in the *spatial* library – (R Development Core Team, 2008) was used in the calculations. Spatial self-correlation was assumed isotropic, since it is one of the main assumptions when including spatial correlation in the GLME models (Pinheiro and Bates, 2000). The Akaike Information Criterion (AIC – Sakamoto, Ishiguro and Kitagawa, 1986) was used for finding the best semi-variogram model. A Gaussian semi-variogram model was choosen for the sedimentation rate, whereas an Exponential semi-variogram model was best for TOC and TN deposition.

## 2.4 Spatial heterogeneity at decreasing spatial scale: site, transect, row and plot

For each study site, ranges of values (maximum – minimum) of TOC (%, $g\,C\,m^{-2}$), TN (%, $g\,N\,m^{-2}$) and sedimentation rates ($kg\,m^{-2}$) were calculated for plot, transect, row and site scales in order to describe spatial variability within study sites (Fig. 2). Plot scale represented 1 $m^2$ portions of each study site (3 pseudo-replicates). Transect and row scales (Fig. 1) were selected to asses the spatial variation of sediment deposition in the direction parallel and perpendicular to the river. As first pointed by Burrough (1996), this anisotropy on spatial variability is often encountered on river systems. Site scale showed spatial variability within sitesm – $j=4$ – with different geomorphological traits. Areas represented by each transect, row and site were identified in the field according to geomorphological traits. Afterwards, the areas were delimitated over 2003 ortho-images using ArcMap 9.2®with a fixed scale of 1:3000, and calculated using the XTools® application. Ranges of values at each scale were calculated taking into account sediment traps enclosed at each of the different spatial scales.

Moreover, two different aspects on the relationship between quantity and composition of deposited sediment were evaluated for each site: i) influence of particle-size separates over TOC (%) and TN (%) concentrations; ii) Influence of particle-size separates over sediment ($kg\,m^{-2}$), TOC ($g\,C\,m^{-2}$) and TN ($g\,N\,m^{-2}$) deposition rates. To accomplish that, Pearson correlations were performed using SPSS®.

## 2.5 Evaluation of the spatial variability at reach scale using GLME modelling

Spatial variability of sediment rate, TOC and TN was assessed at the reach scale using generalized linear mixed-effects (GLME) models. Unlike standard linear models, mixed-effects models allow incorporating both fixed-effects and random-effects in the regression analysis (Pinheiro and Bates, 2000). The fixed-effects in a model describe the values of the response variables in terms of explanatory variables that are considered to be non-random, whereas the random-effects are treated as arising from random causes. Random effects can be associated with the individual experimental units sampled from the population, hence mixed-effects models are particularly suited to experimental settings where measurements are made on groups of related experimental units. If the classification factor is ignored when modelling grouped data, the random (group) effects are incorporated in the residuals, leading to an inflated estimate of the within-site variability.

In our case, relationships were explored between the response variables – Sedrate, TOC and TN – and the covariates – longitudinal and transverse distance to the main channel and percentages of deposited particle size – on a data set grouped according to one classification factor with four levels – the four sampling sites: MP, MD, RF andSF . Hence, the mixed-effects model allows finding relationships between the response variables and the covariates that are general to the four sites, irrespective of the local differences between the sites, which are considered a random effect.

The mixed-effects model combines a random-effects analysis of variance model with a linear regression model. The mathematical formulation takes the form:

$$y_{ji} = \beta_1 + b_j + \beta_2 x_{ji} + \varepsilon_{ji} \quad j = 1,\ldots,4; \quad i = 1,\ldots,201 \tag{1}$$

where $y_{ji}$ is the ith observation in the jth group of data and $x_{ji}$ is the corresponding value of the covariate, an analysis of covariance with a random effect for the intercept; $\beta_1$ is the mean variable value across the population being sampled, $b_j$ is a random variable representing the deviation from the population mean of the mean variable value for the $j$th inter-site study area, and $\epsilon_{ji}$ is a random variable representing the deviation in the mean variable value for observation $i$ on $j$ from the mean variable value for $j$ on $i$.

To complete the statistical model, we must specify the distribution of the random variables $b_{j,}$ $j$=1, . . . , 4 and $\epsilon_{ji,}$ $j$=1, . . . , 4; i=1, . . . , 201. We begin by modelling both of these as independent, normally distributed random variables with mean zero and constant variance. The variances are denoted $\sigma_b^2$ $b_{j,}$ or between site variability, and



HESSD
7, 1589–1619, 2010

$\sigma^2$ for the $\epsilon_{ji,}$ or within-site variability. This is expressed as:

$$b_{j,} \sim N(0,\sigma_b^2), \quad \epsilon_{ji} \sim N(0,\sigma^2) \tag{2}$$

Generalized linear mixed-effects (GLME) models allow including a correlation structure to model the spatial dependence between observations. The inclusion of spatial correlation can be achieved by decomposing the within-group variance-covariance structure – $\epsilon_{ji}$ – into a product of simpler matrices: i) one describing the variance structure of the within-group errors, ii) and the other matrix describing the correlation structure of the within-group errors. The spatial correlation is represented by its semi-variogram; the type of correlation function used to model spatial dependence for Sedrate, TOC and TN corresponds with the best adjustment achieved when modelling their semi-variogram.

The within-group variance-covariance structure – $\epsilon_{ji}$ – in any models assume an homocedastic within-group errors structure, that means that all within-group errors have the same variance. A more general model allows for different variances between study areas and between plots within a study area (heterocedasticity). Heterocedasticity can be included in GLME models by means of a variance function. Heteroscesdasticity was evaluated for all three variables – Sedrate, TOC and TN. Several methods exist for fitting GLME models, including maximum likelihood (ML) and restricted maximum likelihood (REML). The R statistical analysis package – function *lme* from the library *nlme* – (R Development Core Team, 2008) was used for the generalized linear mixed-effectsmodelling. Minimization of the Akaike's Information Criterion was used for selecting the significant covariates (provided by the function *stepAIC* of R), as well as for comparing between homocedastic and heterocedastic models, and between REML and ML fits.

## 3 Results

### 3.1 Spatial heterogeneity at reach scale

Sediment, TOC and TN deposition, as well as related variables (TOC and TN concentration, particle-size separates) showed a high inter-site – $j=4$ – heterogeneity (Table 2). MP presented the highest sediment deposition rate. In turn, the remaining sites presented higher TOC and TN concentrations. Inter-site differences in TOC and TN deposition rates sites diminished when compared with sediment deposition, being the TOC and TN deposition the lowest at RF. With regard to particle-size separates, all fractions <125 µm presented similar inter-site differences than those observed for TOC and TN concentrations, with MP presenting the coarsest deposited sediment. However, particle-size composition was similar between examined sites regarding the <250 and <500 µm particle-size separates.

The relationship between quantity and composition of deposited sediment also presented different trends according to the study site (Table 3). Particle-size separates considered in the study were correlated with sediment, TOC and TN deposited amounts only at RF. At this site, particle-size separates <125 µm were negatively correlated with the amount of sediment deposited. In turn, those separates >125 µm were negatively correlated with the amount of TOC and TN deposited. In addition, no clear patterns were found for the influence on particle-size on TOC and TN concentration at deposited sediments on the different study sites. At MP and RF, TOC and TN concentrations were positively correlated with particle-size separates <125 µm. In turn, TOC and TN concentrations were negatively correlated with the <500 µm particle-size separate at MD, and positively with the <4 µm particle-size separate. In othe words, TOC and TN concentrations increased with decreasing particle-size separate. At SF, the <250 and <500 µm particle-size separate was negatively correlated with TOC and TN content.

Despite the variability added with the pseudo-replicates sampling network, spatial correlation was significant at distances inferior to 0.94 m, 1.30 m, and 1.32 m. for



HESSD

7, 1589–1619, 2010

Spatial variability in floodplain sedimentation

A. Cabezas et al.

Sediment, TOC and TN deposition, respectively (SEDrate, TOCrate, and TNrate in Fig. 2), in all the study area. These results evidenced the need of a 1 $m^2$ sample grid, at least, as the best structure capturing the spatial heterogeneity in the sediment deposition.

### 3.2 Spatial heterogeneity at reach, transect, row and plot scale

In general, it was observed that spatial heterogeneity on all examined variables was as high for longitudinal gradient as it was for the perpendicular gradient (Fig. 3) at all study sites. Moreover, sediment, TOC and TN deposition heterogeneity at plot scale (1 $m^2$) can be as variable as is for parallel and perpendicular gradients which represent bigger areas. However, TOC and TN concentration heterogeneity appeared to be related with the area represented by the considered spatial scales. Focussing in the spatial scales evaluated, it was detected a high degree of intra-scale heterogeneity. For a given study site, the location of either a plot, transect or row determine its variability on depositional rates, as well as for TOC and TN concentrations. Such variability can greatly differ for that observed at other areas within the site when considering similar spatial scales. For example, MP presented for depositional rates the highest difference on heterogeneity between plots, transects and rows, presenting also the highest ranges for all the study sites. However, intra-scale variability was the highest for the remainder sites with regards to TOC and TN concentrations.

### 3.3 Generalized linear mixed-effects modelling

The use of GLME models on the analysis of the sedimentation, TOC and TN deposition rate allowed us to include the four sampling sites in the same analysis, while discriminating between the variance explained by the fixed factors and the random variance depending on the local characteristics of the sites. By doing so we could elucidate which variables were significant in controlling the spatial sedimentation patterns of TOC, TN and deposition rate, independently of the site considered.

At the study reach, the longitudinal distance to superficial water inputs and the perpendicular distance to the main channel decreased the amount of sediment deposited over the floodplain during the examined flood (Table 4). The random effects were large, as reflected by significant differences in the intercept parameter between sampling sites (Table 4). The GLME model for sediment accumulation was the most complex, and included heteroscesdasticity in the model errors, i.e., when grouping the data by the sampling site, resulting in differences in the residuals between sampling sites (Table 4). Best fitting was obtained by ML. No significant effect of particle-size composition over the quantity of deposited sediment was found. In addition, elevation did not have a significant effect.

For TOC and TN, both longitudinal and perpendicular distances were significant, as were the <250 and <500 particle size-classes , with a negative effect on both variables, whereas <4 and <125 µm fractions were although with a positive effect. The random effects were narrower than for the sediment rate, which was reflected by the small variance of between-sites model intercepts (Table 4). The best fit was achieved by REML, and the best models were homocedastic, i.e. the magnitude of the residuals did not change between sampling sites. Neither the <63 µm nor the elevation were estimated as significant and therefore not included in the model.

Coefficients to generate maps of predicted sediment rate, TOC and TN (Fig. 5) were obtained from the GLME models. As expected from the previous description, these maps reflect a high degree of spatial heterogeneity at reach and site scale. As the fixed effects showed, the highest values of deposited sediment, TOC and TN in each sampling site were found close to the main channel and at the upstream end of the site. Differences between sites in the average sediment rate were large, the highest amounts occurring at MP and MD sites whereas lower values were predicted at SF and RF sites. For all sites, the predicted values reflect how sediment deposition decreases when increasing distances both from the main channel and the upstream part, which are the sediment sources.

Regarding to TOC and TN deposition, the spatial patters were similar than for the sediment rate, although the perpendicular distance to the river had a larger importance. Also, the spatial models were a bit more complex than those of the sediment rate, due to the existence in the model of covariates other than the distance to the river. Differences between sampling sites in the mean TOC and TN values were significantly lower than was the case with the sediment rate.

## 4 Discussion

### 4.1 Spatial heterogeneity at different scales

At reach scale, river-floodplain morphology promoted heterogeneity on the amount and composition of sediment released during the examined flood (Table 2). This trend has been previously observed in other studies dealing with contemporary sedimentation rates (Middlekoop and Van der Perk, 1998; Nicholas and Walling, 1998; Thonon et al. 2007). River-floodplain morphology governs hydraulic patterns of overbank flows, and thus sedimentation patterns. Flooding took place later and was intensively shorter at sites with the lower superficial connectivity thresholds (SF and RF in Tables 1 and 2), where sedimentation rates were the lowest. Moreover, a decrease on the amount of suspended sediment during the flood (Asselman and Middlekoop, 1998; Baborowski et al., 2007), which is higher at initial stages, could decrease the amount of sediment deposited at these sites. In turn, the proportion of the finest particle-size separates, i.e. <125 µm (fine sand) increased at those sites. Assuming homogeneity on suspended sediment composition within the study reach, it would result from a drastic decrease of flow velocity at main channel margins. As a result, the coarsest particles, which are normally transported by diffusive processes (Asselman and Middlekoop, 1995; Walling and He, 1998), are released before water enters the floodplain. Such phenomenon could also underlay results at MD, the high-connected side channel. At this site, the amount of sediment deposited was slightly higher than in low-connected sites. Moreover, it was composed by slightly coarser particles. The location of MD in the concave bank of a river meander could reduce the quantity of sediment deposited by increasing erosion at certain flood stages (Steiger and Gurnell, 2003). At the other high-connected site, MP, extraordinary high sedimentation rates of coarse sediment were estimated. This point bar is characterized by a smooth topographic change at the border with the main channel.

Sediment deposition was negatively correlated at reach scale with the proportion of the finest sediment fractions (%<4, 63, 125 µm; $p<0.01$, $n=201$), whereas positively correlated with the %<500 µm particle-size separate ($p<0.01$, $n=201$). However, such trends were only detected at RF when downscaling to site scale (Table 3). Our results, at study site scale, are not in agreement with Steiger and Gurnell (2003) who found a weak negative ($n=108$, $p<0.001$; $r^2=0.320$) relationship between sediment deposited and the <63 µm particle-size separate, although no analysis is provided splitting data by study site. Walling and He (1998), however, showed that these variables were not correlated for some of the sites included in this research. They highlighted the need to recognise that the suspended sediment transported by a river is commonly transported as aggregates rather than individual particles. Results from previous studies emphasized this relationship from the well-developed trend of the coarse fraction to settle close to the river channel due to diffusivity between the main channel and the floodplain, what increased also sediment quantities (Asselman and Midlekoop, 1995; Walling et al., 1997). So, it might also reflect the importance of convective transport processes within the remainder sites (MD, MP, SF).

Oppositely, TOC and TN concentration were at reach scale positively correlated (Table 3) with the proportion of the finest sediment fraction (%<4, 63, 125 µm; $p<0.01$, $n=201$), whereas negatively correlated with the medium sands fraction (%<500 µm; $p<0.01$, $n=201$). Such trends were relatively consistent when down-scaling results to site scale, although the importance of each fraction varied depending on the site. Positive relationships with the percentage of <63 µm particle-size separate have been previously reported (Walling and He, 1997; Steiger and Gurnell, 2003). However, no results are provided for the remainder fractions. In turn, Asselman and Middlekoop (1995) reported different types of organic matter in one site at the Waal River. Particulate organic matter (POM) or light fraction seemed to be deposited at the higher areas, in contrast to fine organic matter which accumulated at low-lying areas. At this site, a clear relationship between spatial patterns of organic matter and particle-size composition of deposited sediments was not found. At the Ebro River study sites, aggregate formation could diminish TOC and TN concentrations at areas with a relatively high proportion of the finer fractions. On the other hand, POM deposition could increase TOC and TN concentrations in areas with a relatively high proportion of the coarser fractions. Future studies should deal with this task by performing particle-size fractionation analysis with no dispersion and/or previous extraction of POM particles.

Within study sites, complexity of local topography creates complex sedimentation patterns (Walling and He, 1998). Spatial differences in sedimentation depend, at first, on the location where water and sediment enter the floodplain. Secondly, local topography attributes as relict channels create preferential flowpaths along which particles and aggregates are conveyed. This results in a decline on sediment deposition along flowpaths (Middelkoop and Van der Perk, 1998). At the examined sites, sediment, TOC and TN deposition varied along gradients which run parallel and perpendicular to the main channel (Fig. 3). Therefore, it is reasonably to assume that deposition from sediment entering the floodplain at the upstream area is as important as that entering adjacent areas to the main channel. Moreover, variability within these gradients can differ depending on the location of the area within the same study site. It implies that either suspended sediment concentrations decreased along flowpaths, or sediment is transported by convective processes further from the input point. Furthermore, heterogeneity was also great at small scales (1 $m^2$). It probably responds to heterogeneous vegetation structure, which modifies flow patterns. Nicholas and Walling (1997) highlighted the need to include such effects on sedimentation modelling in order to improve its predictive ability at small spatial scales. Such variability was smaller at the for TOC and TN concentrations than for the amount of sediment deposited at the Ebro River, reflecting certain homogeneity in the composition of suspended sediments.

### 4.2 Linear mixed-effect models

Using LME models to predict sediment, TOC and TN deposition over riverine floodplains provided a good framework to deal with the high spatial heterogeneity of this phenomenon at different spatial scales. By including the random effect of sampling site and spatial auto-correlation, LME models are able to include the effect of local attributes at different areas within a given river reach. As a result, different coefficients are given for each site to predict Sediment, TOC and TN deposition. Moreover, our approach allowed us handling with small-scale heterogeneity by including all sampling units (pseudo-replicates) at each study plot. Previous studies (Steiger and Gurnell, 2003; Steiger et al., 2003) applied a lumped approach by averaging values of the clustered sampling units. Model inaccuracy belongs, in turn, to the prediction of values at reach-scale by using smaller scale results. Future research should deal with sampling strategies and data analysis techniques in order to increase model accuracy.

According to our models, the amount of deposited sediment, TOC and TN decreases with distance to superficial water inputs (longitudinal and perpendicular distance in Table 4). However, elevation was not considered as a significant variable in any of the models. The inverse correlation of floodplain elevation and sedimentation seems therefore to be masked by the effect of topographic features as levees (Middlekoop and Asselmann, 1998; Thonon et al., 2007). Moreover, high flow velocities at low-lying areas can even reverse this trend at certain flood magnitudes (Asselman and Middlekoop, 1998). The inclusion of the particle size separates in the TOC and TN deposition models reflects the influence that particle-size exerted on sediment composition at the four examined sites. Assignation of model coefficients to the different particle-size classes only respond to the best model goodness of fit. Note that cumulative particle-size fractions were considered for this study.

Spatial patterns of predicted sediment, TOC and TN deposition at each site were therefore dictated by the specific-site location of water and sediment inputs, as well as particle-size composition (Fig. 4). At early flood stages, main channel water enters the point bar (MP) at areas adjacent to the main channel, releasing a large amount of sediment. This process also takes place in the upstream part. The central part of MP is slightly elevated and covered by dense populations of *Tamaryx sp.* and *Populus nigra*. It could create a preferential flowpath in the outer part, reducing sedimentation in upstream areas far from the main channel. Water returns to the main channel at the downstream end of the site, where both flow lines converge, reducing (Middlekoop and Van der Perk, 1998) sedimentation at downstream areas close to the main channel. As a result, particle-size composition of deposited sediments is probably coarser, and TOC and TN deposition not only decreased in the upstream part, where the coarsest sediment is expected, but also in the outer area and at the downstream end, where floodplain water discharges to the main channel.

Processes underlying sedimentation at the remainder sites seems to be similar, although a drastic decrease on flow velocities probably take place at the main channel margin. Such homogeneity on spatial patterns was not expected due to the relatively high topographical complexity of the remainder sites. Flood magnitude and duration probably determined sediment deposition patterns at the examined sites. Also the position of study plots only in areas adjacent to the channel margin could influence the results. Future studies (either during different lower magnitude floods or positioning study plots in areas far to the main channel) are required to elucidate the influence of river discharge on spatial sedimentation patters, which has been previously documented (Asselman and Middlekoop, 1995). At low-connected sites (RF, SF) the presence of dense *Tamaryx sp.* stands possibly reduce flow velocities at areas close to the main channel as much as to promote a higher deposition of either fine sediments or POM exported from the site. It increased higher TOC and TN deposition at these areas even in the downstream part, where predicted deposition rates were relatively low. At the high-connected side channel (MD), either flood magnitude masked the effect of local micro-topography or flow velocities across sites were high enough to decrease TOC and TN concentrations in deposited sediments.

*Acknowledgements.* Field works were funded by the Department of Environmental Science, Technology and University – Government of Aragon (Research group E-61 on Ecological Restoration) – and MEC (CGL2005-07059). The Spanish Research Council (CSIC) granted Álvaro Cabezas through the I3P program (I3P-EPD2003-2), which was financed by European Social Funds (UE). Thanks are extended to Melchor Maestro for his help with the TN analyses. Research of M. Angulo-Martínez is supported by a JAE-Predoc Research Grant from the Spanish National Research Council (Consejo Superior de Investigaciones Científicas—CSIC).

## References

Asselman, N. E. M. and Middelkoop, H.: Floodplain Sedimentation – Quantities, Patterns and Processes, Earth. Surf. Proc. Land., 20, 481–499, 1995.

Asselman, N. E. M. and Middelkoop, H.: Temporal variability of contemporary floodplain sedimentation in the Rhine-Meuse Delta, The Netherlands, Earth. Surf. Proc. Land., 23, 595–609, 1998.

Baborowski, M., Buttner, O., Morgenstern, P., Kruger, F., Lobe, I., Rupp, H., and Von Tumpling, W. V.: Spatial and temporal variability of sediment deposition on artificial-lawn traps in a floodplain of the River Elbe, Environ. Manage., 48, 770–778, 2007.

Buttner, O., Otte-Witte, K., Kruger, F., Meon, G., and Rode, M.: Numerical modelling of floodplain hydraulics and suspended sediment transport and deposition at the event scale in the middle river Elbe, Germany, Acta Hydroch. Hydrob., 34, 265–278, 2006.

Cabezas, A., Comín, F. A., Beguería, S., and Trabucchi, M.: Hydrologic and landscape changes in the Middle Ebro River (NE Spain): implications for restoration and management, Hydrol. Earth Syst. Sci., 13, 273–284, 2009, http://www.hydrol-earth-syst-sci.net/13/273/2009/.

Cabezas, A., Comin, F. A., and Walling, D. E.: Changing patterns of organic carbon and nitrogen accretion on the middle Ebro floodplain (NE Spain), Ecol. Eng., 35, 1547–1558, 2009.

Cabezas, A. and Comin, F. A.: Carbon and nitrogen accretion in the topsoil of the Middle Ebro River Floodplains (NE Spain): Implications for their ecological restoration, Ecol. Eng., in press, 2010.

Day, J. W., Ko, J. Y., Rybczyk, J., Sabins, D., Bean, R., Berthelot, G., Brantley, C., Cardoch, L., Conner, W., Day, J. N., Englande, A. J., Feagley, S., Hyfield, E., Lane, R., Lindsey, J., Mistich, J., Reyes, E., and Twilley, R.: The use of wetlands in the Mississippi Delta for wastewater assimilation: a review, Ocean Coast. Manage., 47, 671–691, 2004.
Heegaard, E. and Nilsen, T.: Local linear mixed effect models - Model specification and interpretation in a biological context, J. Agric. Biol. Envir. S., 12, 414–430, 2007.
Hupp, C. R.: Hydrology, geomorphology and vegetation of Coastal Plain rivers in the southeastern USA, Hydrol. Process., 14, 2991–3010, 2000.
IPCC: Working Group III Report "Mitigation of Climate Change", Cambridge Univeristy Press, Cambridge, UK, 2007.
James, C. S.: Sediment transfer to overbank sections, J. Hydrol. Res., 23, 435–452, 1985.
Johnston, C. A.: Sediment and nutrient retention by freshwater wetlands- Effects on surface-water quality, Crit. Rev. Env. Contr., 21, 491–565, 1991.
Junk, W. J.: The flood pulse concept of large rivers: learning from the tropics, Arch. Hydrobiol., 3, 261–280, 1999.
Knosche, R.: Organic sediment nutrient concentrations and their relationship with the hydrological connectivity of floodplain waters (River Havel, NE Germany), Hydrobiologia, 560, 63–76, 2006.
Middelkoop, H. and Asselman, N. E. M.: Spatial variability of floodplain sedimentation at the event scale in the Rhine-Meuse delta, The Netherlands, Earth Surf. Proc. Land., 23, 561–573, 1998.
Middelkoop, H. and Van der Perk, M.: Modelling spatial patterns of overbank sedimentation on embanked floodplains, Geogr. Ann. A., 80A, 95–109, 1998.
Nicholas, A. P. and Walling, D. E.: Modelling flood hydraulics and overbank deposition on river floodplains, Earth Surf. Proc. Land., 22, 59–77, 1997.
Nicholas, A. P. and Walling, D. E.: Numerical modelling of floodplain hydraulics and suspended sediment transport and deposition, Hydrol. Process., 12, 1339–1355, 1998.
Nicholas, A. P. and Mitchell, C. A.: Numerical simulation of overbank processes in topographically complex floodplain environments, Hydrol. Process., 17, 727–746, 2003.
Noe, G. B. and Hupp, C. R.: Carbon, nitrogen, and phosphorus accumulation in floodplains of Atlantic Coastal Plain rivers, USA, Ecol. Appl., 15, 1178–1190, 2005.
Noe, G. B. and Hupp, C. R.: Retention of Riverine Sediment and Nutrient Loads by Coastal Plain Floodplains, Ecosystems, 12, 728–746, 2009.

Ollero, A.: Dinámica reciente del cauce de el Ebro en la Reserva Natural de los Galachos, Cuat. Geomor., 9, 85–93, 1995.
Owens, P. N., Batalla, R. J., Collins, A. J., Gomez, B., Hicks, D. M., Horowitz, A. J., Kondolf, G. M., Marden, M., Page, M. J., Peacock, D. H., Petticrew, E. L., Salomons, W., and Trustrum, N. A.: Fine-grained sediment in river systems: Environmental significance and management issues, River Res. Appl., 21, 693–717, doi:10.1002/rra.878,, 2005.
Piegay, H., Hupp, C. R., Citterio, A., Dufour, S., Moulin, B., and Walling, D. E.: Spatial and temporal variability in sedimentation rates associated with cutoff channel infill deposits: Ain River, France, Water Resour. Res., 44, W05420, doi:10.1029/2006WR005260, 2008.
Pierce, A. R. and King, S. L.: Spatial dynamics of overbank sedimentation in floodplain systems, Geomorphology, 100, 256–268, 2008.
Pinheiro, J. C. and Bates, D. M.: Mixed-Effects Models in S and S-PLUS, Springer, New York, 530 pp., 2000.
Pizzuto, J. E.: Sediment diffusion during overbank flows, Sedimentology, 34, 301–317, 1987.
Preiner, S., Drozdowski, I., Schagerl, M., Schiemer, F., and Hein, T.: The significance of side-arm connectivity for carbon dynamics of the River Danube, Austria, Freshwater Biol., 53, 238–252, 2008.
Sakamoto, Y., Ishiguro, M., and Kitagawa, G.: Akaike Information Criterion Statistics, Reidel, Dordrecht, Holland, 1986.
Schwarz, G. E.: Estimating the dimension of a model, Ann. Stat., 6, 461–464, 1978.
Steiger, J. and Gurnell, A. M.: Spatial hydrogeomorphological influences on sediment and nutrient deposition in riparian zones: observations from the Garonne River, France, Geomorphology, 49, 1–23, 2003.
Steiger, J., Gurnell, A. M., and Goodson, J. M.: Quantifying and characterizing contemporary riparian sedimentation, River Res. Appl., 19, 335–352, 2003.
Stewart, M. D., Bates, P. D., Price, D. A., and Burt, T. P.: Modelling the spatial variability in floodplain soil contamination during flood events improve chemical mass balance estimates, in: Hihg-Resolution Modelling in Hydrology and Geomorphology, edited by: Bates, P. D. and Lane, S. D., Wiley, Chichester, 239–261, 1999.
Team, R. D. C.: R: A Language and Environment for Statistical Computing, 2008.
Thonon, I., Middelkoop, H., and van der Perk, M.: The influence of floodplain morphology and river works on spatial patterns of overbank deposition, Neth. J. Geosci., 86, 63–75, 2007.

Tockner, K., Pennetzdorfer, D., Reiner, N., Schiemer, F., and Ward, J. V.: Hydrological connectivity, and the exchange of organic matter and nutrients in a dynamic river-floodplain system (Danube, Austria), Freshwater Biol., 41, 521–535, 1999.
Tockner, K., Malard, F., and Ward, J. V.: An extension of the flood pulse concept, Hydrol. Process., 14, 2861–2883, 2000.
Verhoeven, J. T. A., Arheimer, B., Yin, C. Q., and Hefting, M. M.: Regional and global concerns over wetlands and water quality, Trends Ecol. Evol., 21, 96–103, 2006.
Walling, D. E., He, Q., and Nicholas, A. P.: Floodplains as Suspended Sediment Sinks, in: Floodplain Processes, edited by: Anderson, G. M., Walling, D. E., and Bates, P. D., Wiley, Chichester, 399–440, 1996.
Walling, D. E. and He, Q.: Investigating spatial patterns of overbank sedimentation on river floodplains, Water Air Soil Poll., 99, 9–20, 1997.
Walling, D. E., Owens, P. N., and Leeks, G. J. L.: The characteristics of overbank deposits associated with a major flood event in the catchment of the River Ouse, Yorkshire, UK, Catena, 31, 53–75, 1997.
Walling, D. E. and He, Q.: The spatial variability of overbank sedimentation on river floodplains, Geomorphology, 24, 209–223, 1998.
Walling, D. E. and Owens, P. N.: The role of overbank floodplain sedimentation in catchment contaminant budgets, Hydrobiologia, 494, 83–91, 2003.
Walling, D. E.: Quantifying the fine sediment budgets of river basins., Proceedings Irish National Hydrology Seminar, 9–20, 2004.
Witherington, B., Kubilis, P., Brost, B., and Meylan, A.: Decreasing annual nest counts in a globally important loggerhead sea turtle population, Ecol. Appl., 19, 30–54, 2009.



HESSD
7, 1589–1619, 2010



Title Page
Abstract Introduction
Conclusions References
Tables Figures
◀◀ ▶▶
◀ ▶
Back Close
Full Screen / Esc
Printer-friendly Version
Interactive Discussion

**Table 1.** Description of sites where study plots were set.

| Site | Geomorphological feature | Planform setting of channel bank | Surface connectivity ($m^3 s^{-1}$) | Dominant land-cover |
|---|---|---|---|---|
| MP | Point Bar | convex | 350 | Gravel and shrubs |
| MD | Side Channel | concave, natural levee | 400 | Water, grass and trees |
| SF | Side Channel | convex, natural levee | 800 | Water, grass and trees |
| RF | Bench | convex | 600 | Grass and shrubs |



HESSD

7, 1589–1619, 2010

Spatial variability in floodplain sedimentation

A. Cabezas et al.

**Table 2.** One-way ANOVA summary results for deposited sediment variables, grouped by study site. All variables presented significant differences except the <250 µm particle-size. Superscript letters (a, b, c) within a row indicate the sub-groups formed after the applied post-hoc comparisons (SNK or Tahmane Test, $p < 0.05$).

| | Mean ± standar error | | | |
|---|---|---|---|---|
| | MP ($n$=41) | MD ($n$=44) | SF ($n$=44) | RF ($n$=63) |
| Sedrate (Kg m$^{-2}$) | 13.49±2.19$^{a}$ | 5.51±0.53$^{b}$ | 4.18±0.27$^{b}$ | 4.15±0.38$^{b}$ |
| TOC (%) | 0.83±0.05$^{a}$ | 1.51±0.09$^{b}$ | 1.96±0.07$^{c}$ | 1.59±0.07$^{b}$ |
| TN (%) | 0.10±0.01$^{a}$ | 0.18±0.01$^{b}$ | 0.22±0.01$^{c}$ | 0.18±0.01$^{b}$ |
| TOC (g C m$^{-2}$) | 112.49±19.52$^{a}$ | 77.26±7.91$^{b}$ | 78.93±4.08$^{b}$ | 56.13±4.36$^{b}$ |
| TN (g N m$^{-2}$) | 11.56±1.67$^{a}$ | 8.79±0.83$^{b}$ | 9.10±0.46$^{b}$ | 6.36±0.44$^{c}$ |
| <4 µm (%) | 2.83±0.16$^{a}$ | 4.27±0.22$^{b}$ | 5.53±0.26$^{c}$ | 4.19±0.22$^{b}$ |
| <63 µm (%) | 24.01±1.43$^{a}$ | 32.67±1.43$^{b}$ | 40.44±1.39$^{c}$ | 31.11±1.24$^{b}$ |
| <125 µm (%) | 43.75±2.20$^{a}$ | 50.37±1.78$^{b}$ | 57.62±1.45$^{c}$ | 48.85±1.30$^{b}$ |
| <250 µm (%) | 74.49±1.84 | 71.46±1.86 | 74.57±1.39 | 71.34±1.03 |
| <500 µm (%) | 92.88±0.69$^{a}$ | 88.90±1.27$^{b}$ | 88.96±0.90$^{b}$ | 88.56±0.76$^{b}$ |



HESSD

7, 1589–1619, 2010

Spatial variability in floodplain sedimentation

A. Cabezas et al.

HESSD
7, 1589–1619, 2010



**Table 3.** Bivariate correlation between sediment particle-size, carbon and nitrogen concentration and deposition rates (sediment, TOC and TN). Data has been separated by study site: RF, MP; SF, MD. For an easier interpretation, correlations not related to the investigated aspects (see methods) are not displayed.

| | | RF | | | | | | | | | |
|---|---|---|---|---|---|---|---|---|---|---|---|
| | | SEDrate | TOC | TN | TOCrate | TNrate | 4 µm | 63 µm | 125 µm | 250 µm | 500 µm |
| MP | SEDrate ($Kg\,m^{-2}$) | | – | – | – | – | −0.45** | −0.49** | −0.43** | −0.24 | −0.23 |
| | TOC (%) | – | | – | – | – | 0.53** | 0.43** | 0.25* | −0,11 | −0,30* |
| | TN (%) | – | – | | – | – | 0.61** | 0.52** | 0.34** | −0.02 | −0.20 |
| | TOCrate ($g\,C\,m^{-2}$) | – | – | – | | – | −0.15 | −0.22 | −0.25* | −0.35** | −0.52** |
| | TNrate ($g\,N\,m^{-2}$) | – | – | – | – | | −0.15 | −0.21 | −0.23 | −0.31* | −0.47** |
| | %<4 µm | −0.13 | 0.57** | 0.52** | 0.04 | 0.05 | | – | – | – | – |
| | %<63 µm | −0.16 | 0.55** | 0.48** | 0.01 | 0.02 | – | | | – | – |
| | %<125 µm | −0.13 | 0.55** | 0.43** | 0.04 | 0.05 | – | – | | – | – |
| | %<250 µm | 0.15 | 0.45** | 0.16 | 0.25 | 0.27 | – | – | – | | – |
| | %<500 µm | 0.27 | 0.21 | −0.04 | 0.23 | 0.27 | – | – | – | – | |
| | | SF | | | | | | | | | |
| | | SEDrate | TOC | TN | TOCrate | TNrate | 4 µm | 63 µm | 125 µm | 250 µm | 500 µm |
| MD | SEDrate ($Kg\,m^{-2}$) | | – | – | – | – | −0.07 | −0.01 | 0.10 | 0.23 | 0.25 |
| | TOC (%) | – | | – | – | – | −0.07 | −0.24 | −0.38* | −0.54** | −0.63** |
| | TN (%) | – | – | | – | - 0.21 | 0.01 | −0.19 | −0.39** | −0.48** | |
| | TOCrate ($g\,C\,m^{-2}$) | – | – | – | | – | −0.03 | −0.09 | −0.09 | −0.06 | −0.09 |
| | TNrate ($g\,N\,m^{-2}$) | – | – | – | – | | 0.11 | 0.06 | 0.05 | 0.06 | 0.06 |
| | %<4 µm | −0.05 | 0.33* | 0.31* | 0.17 | 0.22 | | – | – | – | – |
| | %<63 µm | −0.06 | 0.24 | 0.25 | 0.13 | 0.19 | – | | – | – | – |
| | %<125 µm | 0.06 | 0.07 | 0.07 | 0.17 | 0.23 | – | – | | – | – |
| | %<250 µm | 0.13 | −0.19 | −0.19 | 0.11 | 0.17 | – | – | – | | – |
| | %<500 µm | 0.13 | −0.38* | −0.37* | 0.00 | 0.06 | – | – | – | – | |

**= Correlation is significant at the 0.01 level (2-tailed).
*= Correlation is significant at the 0.05 level (2-tailed).

**Table 4.** Summary of the results of the generalized linear mixed-effects models for sedimentation rate (SEDrate), Total Organic Carbon (TOCrate) and Total Nitrogen (TNrate): Goodness of fit statistic value (AIC); Fitting method: Maximum Likelihood (ML) or Restricted Maximum Likelihood (REML); Correlation parameters; Random effects for sampling site and model corresponding to the intercept and, in the case of heterocedasticity, in the residuals; Coefficients of the fixed effects: Coeff., Beta Coeff. (standarized coefficients) and p-values for the sedimentation rate (SEDrate), Total Organic Carbon (TOCrate) and Total Nitrogen (TNrate) models. Long. Dis. = Longitudinal distance; Perp. Dis. = Perpendicular distance (see methods for details).

| | SEDrate | TOCrate | TNrate |
|---|---|---|---|
| AIC | 947.21 | −488.72 | −1424.18 |
| Fitting method | ML | REML | REML |
| Correlation parameters | | | |
| Range | 1.183 | 0.897 | 0.898 |
| Nugget | 0.222 | 2.87E-10 | 8.29E-09 |
| Random effects (per sampling site) | | | |
| Intercept | | | |
| MP | 13.645 | 0.322 | 0.028 |
| MD | 11.295 | 0.296 | 0.027 |
| RF | 8.110 | 0.285 | 0.026 |
| SF | 7.224 | 0.260 | 0.023 |
| Residual | | | |
| MP | 42.776 | | |
| MD | 12.714 | | |
| RF | 4.260 | 0.064 | 0.006 |
| SF | 3.991 | | |

| Fixed effects | SEDrate Coeff. | SEDrate Beta Coeff. | SEDrate p-value | TOCrate Coeff. | TOCrate Beta Coeff. | TOCrate p-value | TNrate Coeff. | TNrate Beta Coeff. | TNrate p-value |
|---|---|---|---|---|---|---|---|---|---|
| Long. Dis. | −0.01722 | −1.7184 | 0.0000* | −0.00016 | −0.01622 | 0.0223* | −0.00002 | −0.00184 | 0.0041* |
| Perp. Dis. | −0.05512 | −1.1337 | 0.0000* | −0.00084 | −0.01722 | 0.0185* | −0.00007 | −0.00146 | 0.0264* |
| %<4 µm | – | – | – | 0.01310 | 0.02420 | 0.0152* | 0.00108 | 0.00200 | 0.0251* |
| %<125 µm | – | – | – | −0.00387 | −0.04833 | 0.0065* | −0.00031 | −0.00393 | 0.0135* |
| %<250 µm | – | – | – | 0.00547 | 0.05634 | 0.0037* | 0.00048 | 0.00500 | 0.0041* |
| %<500 µm | – | – | – | −0.00467 | −0.03104 | 0.0100* | −0.00040 | −0.00269 | 0.0129* |

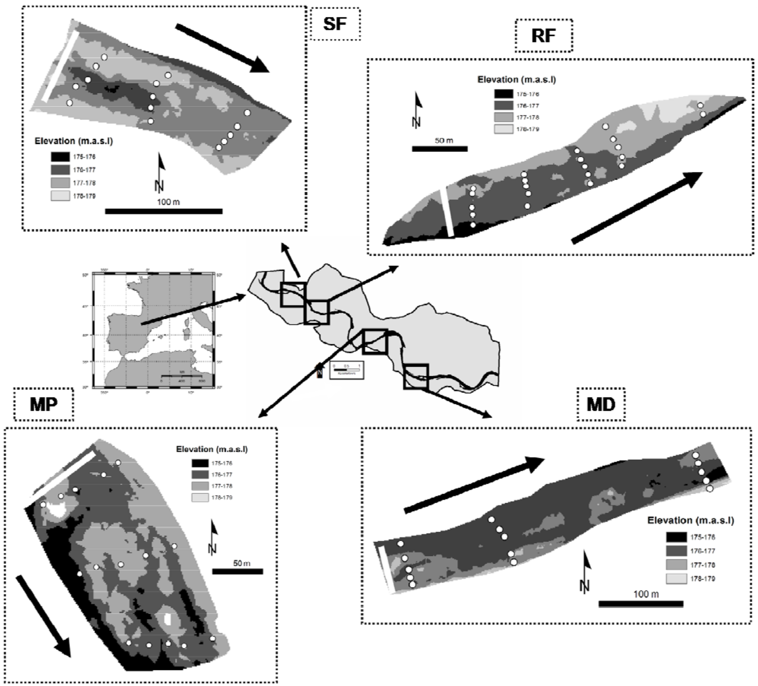


**Fig. 1.** Location of study plots along the four sites selected within the study reach, which are represented by a detailed Digital Elevation Model. Black arrows indicate the direction of the Ebro River flow. White circles represent the location of the study plots, reflecting an incremental distance to main channel along a perpendicular gradient. White solid lines at each site represent the area where surface water inputs the site, which has been the reference to calculate distances along a longitudinal gradient (see methods).

HESSD
7, 1589–1619, 2010

Spatial variability in floodplain sedimentation

A. Cabezas et al.

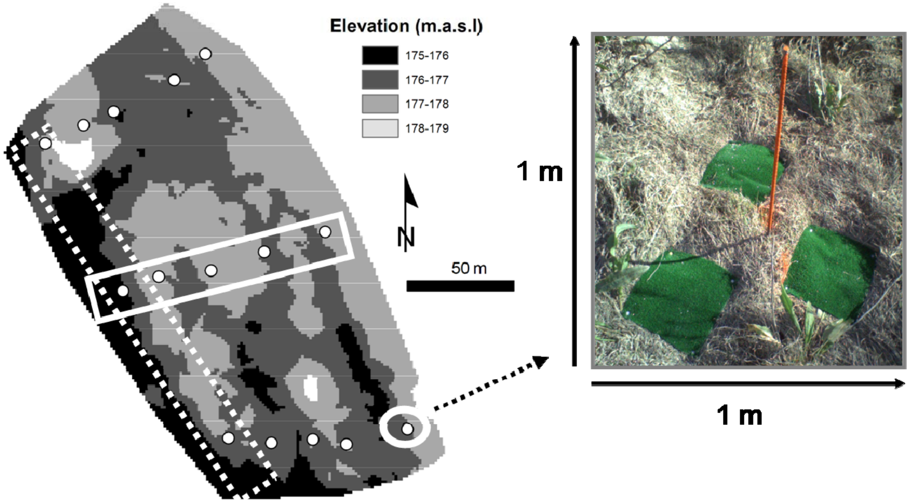


**Fig. 2.** Representation of the different spatial scales considered in one of the examined areas (MP, see Fig. 1). The biggest one, the study site scale, encounters the area containing all study plots within a site. The solid rectangle is an example of the area encountered by transects spatial scale, which represents the gradient perpendicular to the main channel. The dashed rectangle is an example of the area encountered by the row spatial scale, which represents the gradient parallel to the main channel. The displayed picture shows the composition of one study plot (solid circle).



HESSD
7, 1589–1619, 2010



Title Page
Abstract Introduction
Conclusions References
Tables Figures
◂◂ ▸▸
◂ ▸
Back Close
Full Screen / Esc
Printer-friendly Version
Interactive Discussion

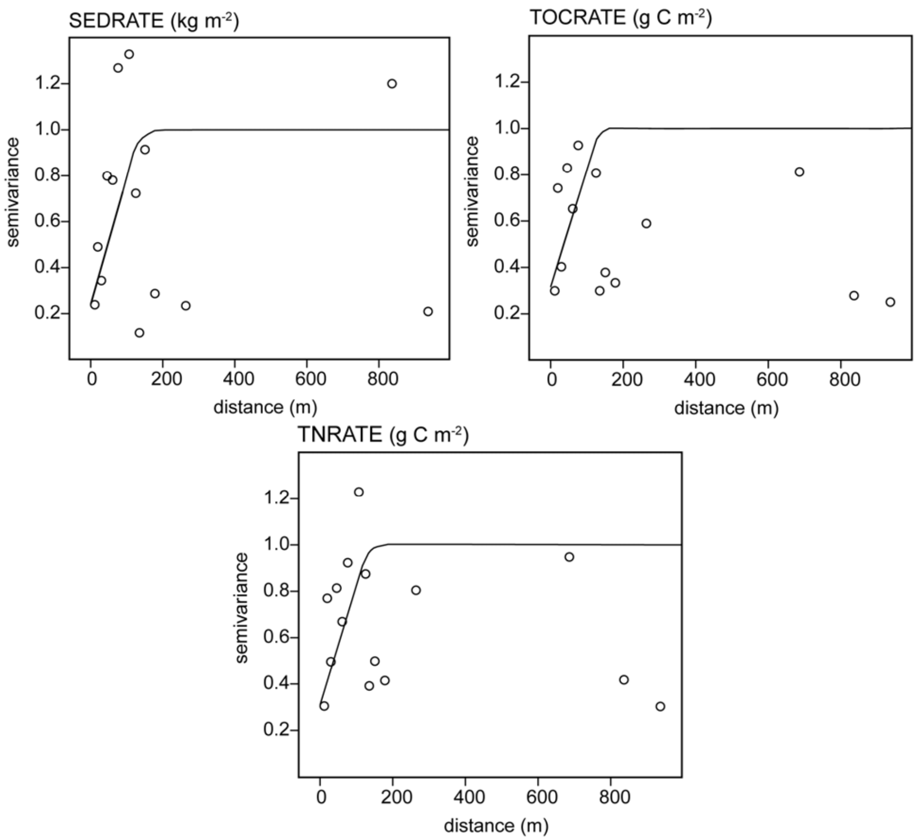


**Fig. 3.** Empirical semivariograms (circles) and fitted Gaussian and Exponential semivariogram models (lines) of the Sediment, TOC and TN deposition at one study reach of the Middle Ebro River. Range parameters are: 0.9414 m. for Sedrate, 1.2963 m. for TOCrate, and 1.3242 m. for TNrate.



HESSD

7, 1589–1619, 2010

Spatial variability in floodplain sedimentation

A. Cabezas et al.

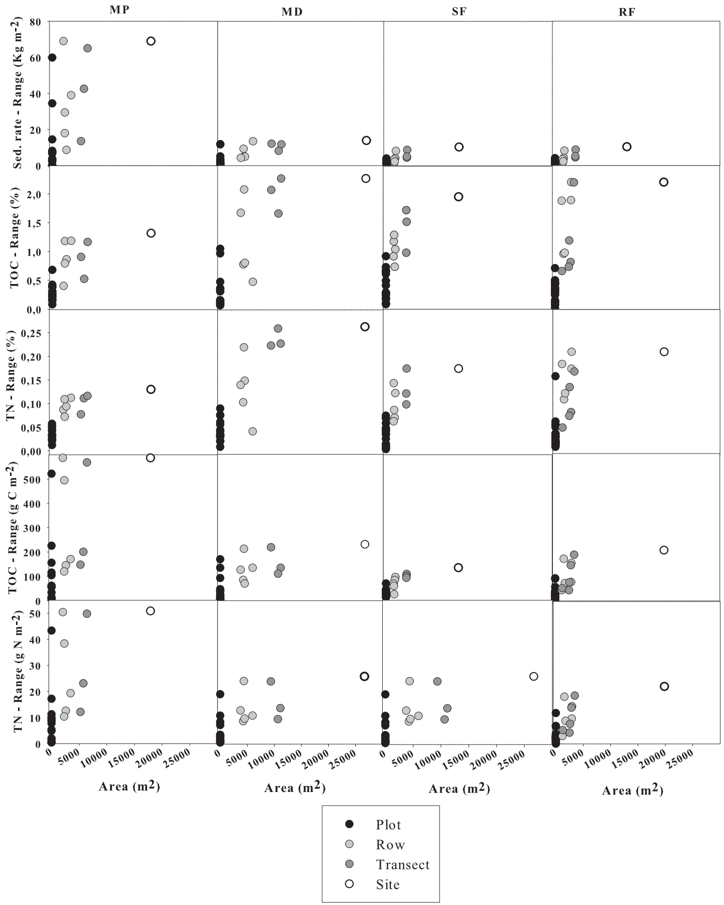


**Fig. 4.** TOC (%, $g\,C\,m^{-2}$), TN (%, $g\,N\,m^{-2}$) and sedimentation rates ($kg\,m^{-2}$) ranges for different spatial scales (plot, transect, row and site). See methods for details on area calculations.



HESSD

7, 1589–1619, 2010

Spatial variability in floodplain sedimentation

A. Cabezas et al.

HESSD
7, 1589–1619, 2010



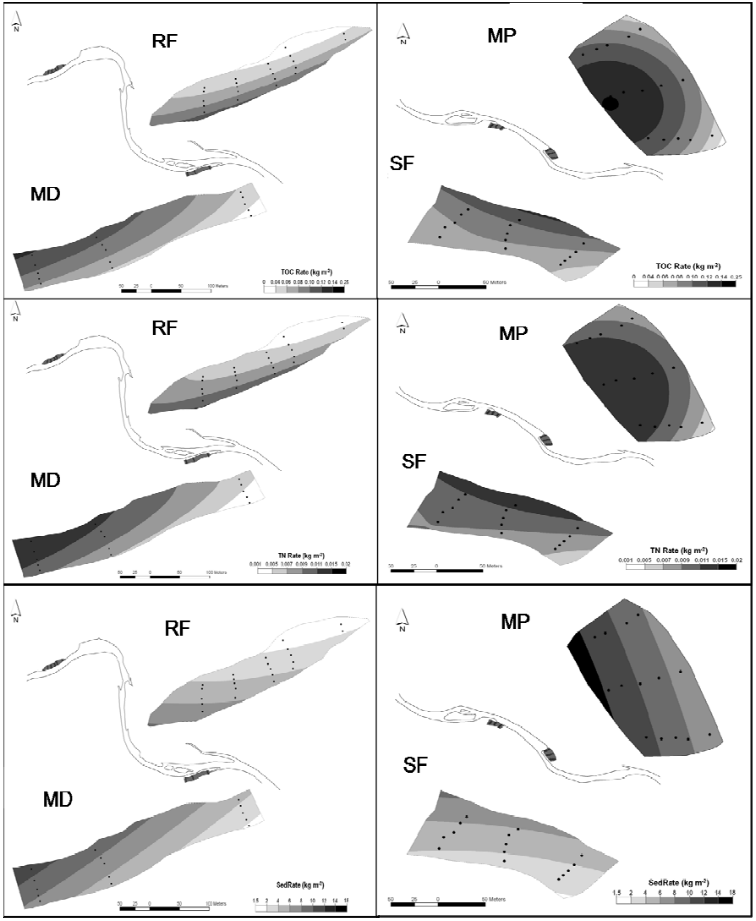


**Fig. 5.** Prediction maps sediment, TOC and TN deposition after the Generalized linear mixed-effects models.